

A. Camero Arranz\*, P. Reig\*, P. Connell\*, S. Martínez Núñez\*, P. Blay\*, V. Beckmann†, and V. Reglero\*

\*GACE, Instituto de Ciencias de los Materiales, Universidad de Valencia, P.O. Box 22085, 46071 Valencia, Spain

†NASA Goddard Space Flight Center, Code 661, Greenbelt, MD 20771, USA

## ABSTRACT

We have performed a data analysis of the high-mass X-ray binary EXO 2030+375 using the three high-energy instruments on board *INTEGRAL* during a normal outburst of the source. The observations were made during the *INTEGRAL* Performance Verification phase in December 2002 and represent a total on-source time of about  $10^6$  s. X-ray pulsations with a pulse period of  $41.64 \pm 0.07$  s are detected with both JEM-X and ISGRI instruments, in agreement with previous results. The 10–200 keV spectrum can be fitted with a power law model yielding  $\Gamma = 2.54^{+0.14}_{-0.04}$  or with a bremsstrahlung model with  $kT = 34^{+4}_{-3}$  keV. A four-day delay between periastron passage and the peak of the outburst is found.

Key words: binary systems – BeX – HMXBs – EXO 2030+375.

## 1. INTRODUCTION

EXO 2030+375 is a Be/X-ray binary, i.e. a neutron star orbiting a Be companion (Coe 2000). X-rays are produced when matter from the circumstellar disk of the Be star is accreted onto the surface of the neutron star. Given the relatively high eccentricity of Be/X-ray binaries, accretion normally takes place during periastron passages. So recurrent outbursts modulated with the value of the orbital period are normally observed. These are known as type I outbursts. Sometimes, a much brighter outburst (type II), normally associated with a high activity at other wavelength bands, is detected. They do not correlate with the orbital period and are accompanied by strong spin-up episodes (Bildsten et al. 1997).

EXO 2030+375, with an orbital period of  $P_{\text{orb}} = 46.0214 \pm 0.0005$  d and an eccentricity of  $e = 0.419 \pm 0.002$  (Wilson et al., 2002), was discovered by *EXOSAT* in 1985 during a type II X-ray outburst (Parmar et al. 1989). The X-ray luminosity in the energy range 1 – 20 keV reached a value of  $L_x \sim 10^{38}$  erg s $^{-1}$ . Since then, only type I outbursts, showing strong orbital modulation and  $L_x < 10^{37}$  erg s $^{-1}$  have been detected.

The optical and infrared emission is dominated by the Be star and characterised by spectral lines in emission (particularly those of the Balmer series) and IR excess (Reig & Coe 1998). The optical counterpart of EXO 2030+375 is a very reddened main-sequence star, with a visual magnitude of 20 and spectral type B0 (Motch & Janot-Pacheco 1987; Coe et al. 1988).

In the X-ray band the source shows pulsations with a period of 41.7 s (Parmar et al. 1989; Reynolds, Parmar & White 1993, Reig & Coe 1998). The continuum spectral shape of EXO 2030+375 in the 2–20 keV energy range has been represented by a power law function ( $\Gamma = 1.00 \pm 0.06$ ), with an exponential cut-off ( $\sim 8.85 \pm 0.33$  keV), coupled with low-energy absorption ( $N_H = 2.6 \pm 0.3 \times 10^{22}$  cm $^{-2}$ ) and an iron emission line at  $\sim 6.5$  keV (Reig & Coe 1999). In the energy range of 20–100 keV, a thermal bremsstrahlung was the best-fitting model ( $kT = 20.2 \pm 0.3$  keV) obtained using BATSE data by Stollberg et al. (1999).

In this paper we present a detailed imaging, spectral and timing analysis of EXO 2030+375 during *INTEGRAL* Performance and Verification Phase. Preliminary results of EXO 2030+375 made with *INTEGRAL* have been reported in Martínez Núñez et al. (2003), Kuznetsov et al. (2003; 2004) and Bouchet et al. (2003). This work, however, represents the first time that a combined analysis using all three high-energy instruments onboard *INTEGRAL* is carried out.

## 2. OBSERVATIONS AND DATA REDUCTION

The **INTE**rnational **GA**mma-**RA**y **AS**trophysics **L**aboratory (*INTEGRAL*, Winkler et al. 2003) consists of three coded mask telescopes, the spectrometer SPI (20 keV–8 MeV), the imager IBIS (15 keV–10 MeV), and the X-ray monitor JEM-X (3.5–35 keV), as well as the optical monitoring camera OMC (V, 500–600 nm).

IBIS with an angular resolution of 12 arcmin and a fully coded field of view of  $9 \times 9$  deg (partially coded  $29 \times 29$  deg), provides accurate source identification, good spatial sensitivity and fine imaging capabilities. It consists of two layers, the top one is made of CdTe solid-state detectors (ISGRI), and the bottom one contains CsI scintillator

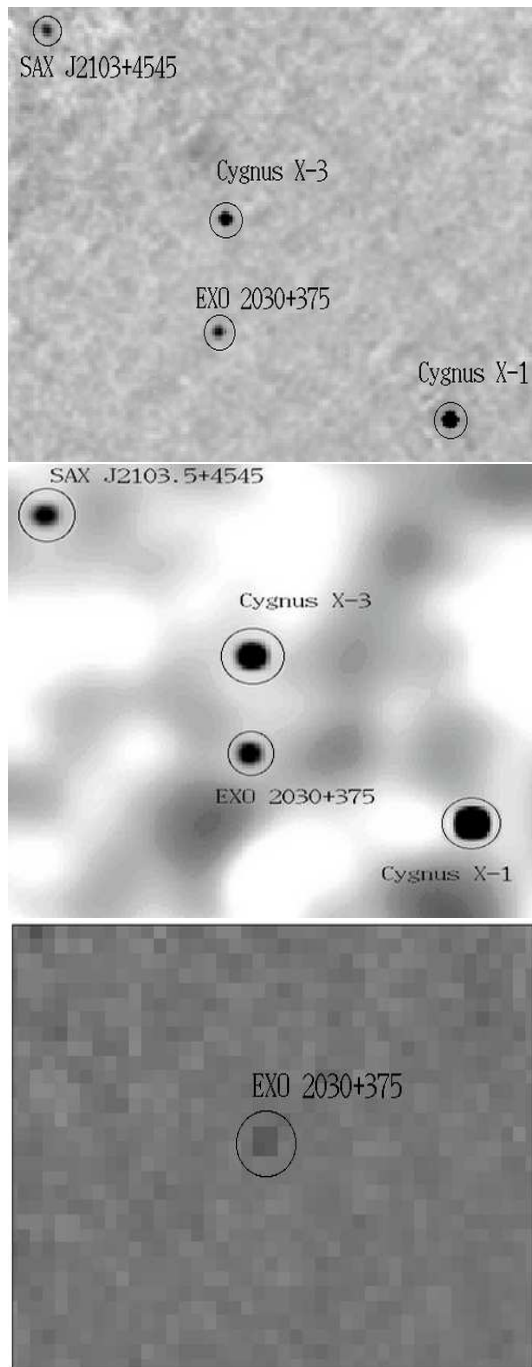


Figure 1. Top: A mosaic of the Cygnus region by ISGRI detector, corresponding to revolution 20. Middle: SPI average image from revolutions 19 to 23. Bottom: JEM-X (detector 2) image of EXO 2030+375, from ScW 001900400010.

crystals (PICsIT) (Ubertini et al. 2003). The SPI spectrometer provides a good angular resolution of 2.6 deg (however point sources can be located within few arcminutes) and an excellent energy resolution (2.35 keV at 1.33 MeV). Nineteen cooled, hexagonal Germanium modules, with a total area of 500 cm<sup>2</sup>, compose this detector (Vedrenne et al. 2003). The JEM-X monitor consists of two identical coded-aperture mask telescopes co-aligned with the other instruments. The detectors are microstrip gas chambers with a collecting area of 500 cm<sup>2</sup> per unit. It was designed to work in the energy range 3-35 keV with an energy resolution of  $\Delta E/E = 0.47 \times (E/1\text{keV})^{-1/2}$  and a timing resolution of 122  $\mu\text{s}$  (Lund et al. 2003).

The analysed data of the present work have been obtained during the *INTEGRAL* performance verification (PV) phase. This phase covers the period from October 17, 2002 (launch) to the end of December 2002. EXO 2030+375 is located in the Cygnus region near two strong gamma-ray sources, Cygnus X-1 and Cygnus X-3, and a weaker one, SAX J2103.5+4545 (Blay et al. 2004). During the revolutions 19 to 22 (6-15 December 2002, 52618–52628 MJD) a type I outburst of EXO 2030+375 was observed.

Because the diameter of the spectrometer detector array is smaller than that of its coded mask, and each detector has a large width, *SPI* cannot get sufficient information for imaging with just one exposure like the other instruments on *INTEGRAL* but needs to make a number of exposures around a source direction, each shifted by about 2.0 degrees in a so called *dithering* pattern, usually consisting of a 5x5 array of pointing directions.

*INTEGRAL* performed nearly 450 pointings around the Cygnus region containing EXO 2030+375 throughout the duration of its outburst, but there are effectively only about 75 *independent* pointings, due to sequences of 5x5 dithering patterns being repeated at the same location. If a dot is placed on a sky map for each of the 450 exposure directions only about 75 can be seen due to overlapping. Because of this we have a reduced no of *independent* exposures which limits the ability of *SPI* to distinguish between sources in its field of view. Given the large positive and negative side lobe structure in the point spread function of *SPI* this will limit the resolution of weak sources and introduce more significant artefacts in the residue images.

In the majority of these pointings EXO 2030+375 was outside the JEM-X field of view (about 90%). In contrast, for ISGRI/IBIS we were able to detect the source in almost all the pointings. However, for the timing analysis we have taken into account only those pointings with detection level above  $8\sigma$ . For the spectral analysis we considered only observations that fell inside the fully coded field of view. SPI data cover all the outburst, that is, near 10 days.

Data reduction was carried out with ISDC's (Courvoisier et al. 2003) Offline Scientific Analysis software, release 3.0. Software description can be found in Goldwurn et al. (2003), Diehl et al. (2003), and Westergaard et al. (2003).

Table 1. Journal of Observations

Instrument	Rev	Obs.Time ks	Mean Flux phot cm <sup>-2</sup> s <sup>-1</sup> keV <sup>-1</sup>
JEM-X 2	19	9	$(11.3 \pm 0.4) \times 10^{-4}$
JEM-X 1 (10-25 keV)	19/20	13	$(15.2 \pm 0.3) \times 10^{-4}$
ISGRI/IBIS (20-45 keV)	19	120	$(2.4 \pm 0.9) \times 10^{-4}$
	20	150	$(3.3 \pm 0.7) \times 10^{-4}$
	21	80	$(2.7 \pm 0.4) \times 10^{-4}$
	22	10	$(2.0 \pm 0.5) \times 10^{-4}$
SPI (40-100 keV)	19	180	$(2.5 \pm 0.9) \times 10^{-5}$
	20	160	$(8 \pm 1) \times 10^{-5}$
	21	50	$(11 \pm 2) \times 10^{-5}$
	22	170	$(4 \pm 1) \times 10^{-5}$
	23	170	$(2 \pm 0.3) \times 10^{-5}$

### 3. DATA ANALYSIS

#### 3.1. Imaging

Figure 1 shows the images obtained with the three high-energy instruments on board *INTEGRAL*. ISGRI detected EXO 2030+375 during revolutions 19 to 22. The total observing time was 360 ks, obtaining the best location at R.A.=308.09° and DEC=37.65°, with a 0.03° error radius. SPI detected this source (total observing time 680 ks) from revolutions 19 to 23, with a statistical significance of 35σ, at R.A.=308.12±0.07° and DEC=37.46±0.05°. JEM-X has the smallest fully coded field of view (4.8°), and it was possible to localise the source in 13 pointings of revolution 19 and 20 (total observing time 21 ks). Best JEM-X location is R.A.=308.06° and DEC=37.64° with an error radius of 0.03°, and the best detection was found in ScW 001900400010.

The flux trend obtained by the imaging analysis, averaged on a revolution basis (see Tab.1), is in agreement, as expected, with what is obtained by the timing analysis (Fig.3). Namely, an increase by a factor of ~ 3 from revolution 19 up to 20, a peak at around MJD 52622 and a decrease in approximately the same period of time as the rise, up to revolution 23.

#### 3.2. Timing

EXO 2030+375 exhibits variability on all time scales. In the short-term the X-ray emission is characterised by pulsations. Our JEM-X and IBIS/ISGRI data analysis confirms the periodicity. In order to derive a value of the pulse period we employed two techniques. A Fast Fourier Transformation on the 5-s binned ISGRI light curve (energy range 20–40 keV) corresponding to the science window 00190041 revealed a peak at 0.024 Hz. This value of the spin period is in good agreement with previous results (Parmar et al. 1989, Reynolds et al. 1993, Reig & Coe 1998). In addition, we used epoch-folding analysis for

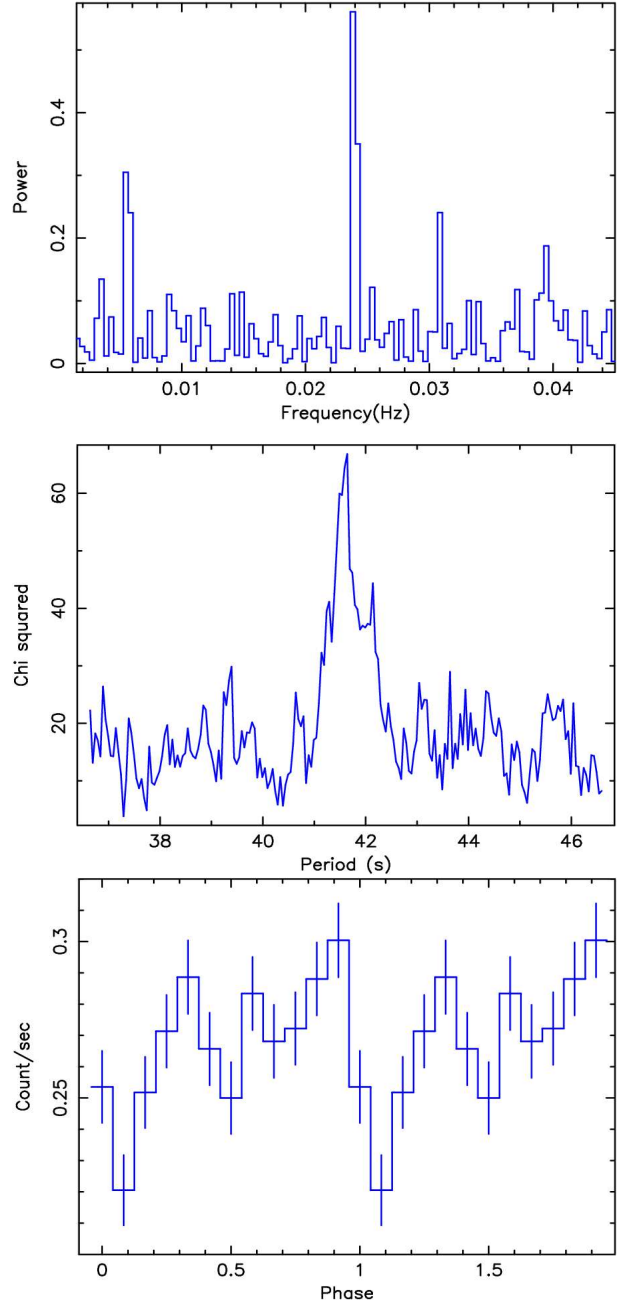


Figure 2. Results of the Fourier analysis on ISGRI SWID=001900410010 light curve (top), and epoch-folding analysis on JEM-X data (middle) (d.o.f.= 11). On the bottom, the time-averaged pulse profile. A pulse period of  $41.64 \pm 0.07$  s is derived.

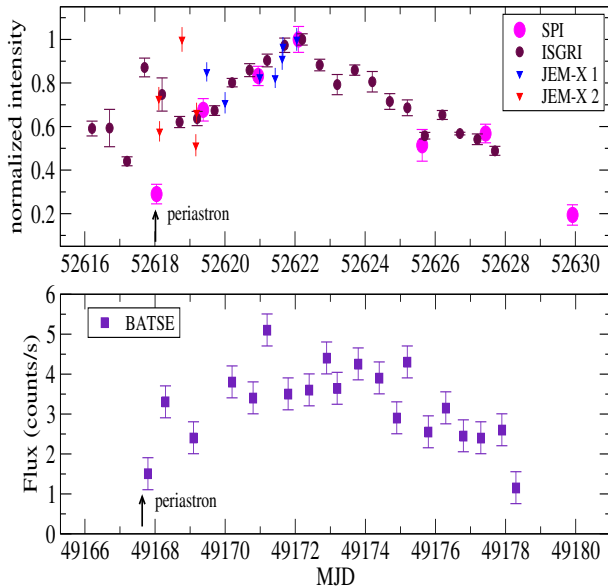


Figure 3. JEM-X (9–25keV), ISGRI and SPI (20–40keV) light curves (top), and an old outburst detected by BATSE (20–50 keV) (bottom). JEM-X, ISGRI and SPI data were normalised together for a better comparison, the peak value was taken as unity of measurement.

JEM-X data (energy range 4–25 keV) obtaining an averaged pulse period of  $41.64 \pm 0.07$  s (without barycentric corrections due to software limitations) (Fig. 2). The error of this pulse was determined by the standard deviation of the different values obtained from each measurement.

In the medium-term EXO 2030+375 shows type I outbursts, i.e., increases of the X-ray flux during the periastron passage of the neutron star. Fig. 3 shows a comparison of the (10–25 keV) JEM-X, (20–40keV) ISGRI and SPI light curves from revolutions 19 to 23, with that of an old outburst detected by BATSE (20–50 keV)(Reig & Coe 1998). We can see that the duration of the outburst (about 10 days), the shape of the outburst and the amplitude of variability are very similar, indicating that the geometrical and the accretion parameters at the periastron are stable through the years. In addition, it is important to note that there is a four-day delay between the maximum of luminosity and the periastron passage of the neutron star in all light curves. Previous results showed that EXO 2030+375’s outbursts shifted from peaking about 6 days after periastron to peaking before periastron (Wilson et al., 2002).

### 3.3. Spectral analysis

The data from different instruments can, in principle, be combined to attain a broad-band spectrum from 3 keV to 1 MeV, with the capabilities of one instrument being complementary to the other ones. However, in practice, the present limitations of the software, the preliminary of the calibration (Lubiński et al. 2004), observational constraints and the weakness of the source constrain the amount of information that can be extracted.

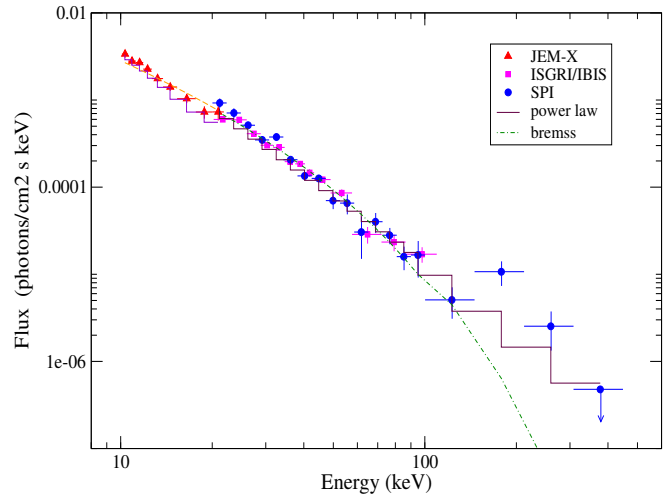


Figure 4. Combined JEMX-ISGRI-SPI mean spectrum of EXO 2030+375.

The amount of data varies according to the instrument characteristics. For JEM-X we obtained an average spectrum in the energy range 10–25 keV by using five Science Windows of revolution 19. Only observations in which the source lied inside the ISGRI/IBIS fully coded field of view were used for the spectral analysis ( 20%), which implies that there are no spectral data for revolutions 21 to 23. Therefore, the average ISGRI spectrum was built using 35 spectra from revolutions 19 and 20.

SPI has the largest field of view, hence EXO 2030+375 was detected throughout the entire duration of the outburst (revolutions 19 to 23). For this instrument, however, the main constraints stem from the relatively high background. In order to improve the signal to noise, an average spectrum combining all observations was necessary.

A single power-law model has been fitted to all *INTEGRAL* data simultaneously. The spectral parameters corresponding to the best-fit power-law model are given in Table 2. For ISGRI and SPI, a thermal bremsstrahlung model with  $kT \approx 34$  keV also provided acceptable fits. Systematic uncertainties were added on JEM-X (5%) and ISGRI/IBIS (10%) spectra.

The mean photon indexes of the three instruments are in good agreement (within the error bars). In Figure 5 we plotted SPI spectral indices per revolution as a function of flux. There seems to be a hardening of the spectrum as the flux increases, although it is not statistically significant (the power law indexes have big uncertainties because the spectra per revolution have poor signal to noise ratios).

Finally, a 10-200 keV broad-band spectrum has been obtained joining the mean-spectra of each instrument ( Figure 4 ). A power law model with  $\Gamma = 2.54^{+0.14}_{-0.04}$  provided a good fit. Also the combined spectrum can be well fitted with bremsstrahlung model with  $kT = 34^{+4}_{-3}$  keV. However, this model clearly deviates at energies above 100 keV. A summary of the intercalibration factors for both models is shown in Table 3. ISGRI and SPI normalization is con-

Table 2. Results of the spectral analysis

Instrument	Rev	Photon index	$\chi_r^2/dof$	Flux ( $\times 10^{-10}$ ) erg cm $^{-2}$ s $^{-1}$	kT keV	$\chi_r^2/dof$	Flux ( $\times 10^{-10}$ ) erg cm $^{-2}$ s $^{-1}$
JEM-X 2 (10-25 keV)	19	2.4 $\pm$ 0.3	0.9/65	4.2	–	–	–
IBIS (20-100 keV)	19	2.7 $\pm$ 0.1	0.9/24	6.2	–	–	–
	20	2.5 $\pm$ 0.1	0.8/24	7.1	–	–	–
average spectrum		2.63 $\pm$ 0.14	0.9/24	6.3	33 $^{+8}_{-4}$	0.9/24	6
SPI (20-200 keV)	19	3.3 $\pm$ 0.3	0.8/15	7.5	–	–	–
	20	3.0 $\pm$ 0.2	1.5/15	11	–	–	–
	21	2.0 $\pm$ 0.5	0.5/15	12	–	–	–
	22	2.9 $\pm$ 0.4	1.5/15	8.5	–	–	–
	23	2.6 $\pm$ 0.3	2.7/15	8.2	–	–	–
average spectrum		2.81 $\pm$ 0.16	1.5/15	7.2	30 $\pm$ 5	2.4/15	6.24

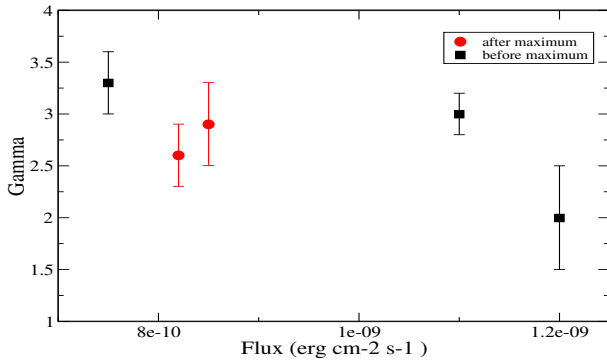


Figure 5. SPI spectral indexes per revolution as a function of flux.

sistent with each other. On the other hand, no cutoff at 200-300 keV, as seen in black-hole systems, seems to be present although the data is not conclusive. The average X-ray luminosity was  $3.8 \times 10^{36}$  erg s $^{-1}$ , for an assumed distance of 5 kpc (Parmar et al. 1989). This luminosity value is of the same order as previous type I outbursts of this source.

#### 4. CONCLUSIONS

We have analysed data from the three high-energy instruments on board *INTEGRAL* of the high-mass X-ray binary EXO 2030+375 during an outburst which took place during PV phase. X-ray pulsations with a pulse period of  $41.64 \pm 0.07$  s were clearly detected in JEM-X and ISGRI light curves. The averaged 10-200 keV spectrum can be described by a single power law model with a photon index of  $2.54^{+0.14}_{-0.04}$  or by thermal bremsstrahlung of temperature  $34^{+4}_{-3}$  keV. The average X-ray luminosity in this energy range was  $3.8 \times 10^{36}$  erg s $^{-1}$ , assuming a distance of 5 kpc, in agreement with previous type I outburst of this source.

Table 3. Broad-band spectral parameters (10–200 keV).

Photon index	$\chi_r^2/dof$	Flux (erg cm $^{-2}$ s $^{-1}$ )	Intercalibration factors (ISGRI/JEM-X SPI/JEM-X)
$2.54^{+0.14}_{-0.04}$	1.25/100	$1.2 \times 10^{-9}$	$1.42^{+0.3}_{-0.07}$ $1.50^{+0.3}_{-0.1}$
kT (keV)	$\chi_r^2/dof$	Flux (erg cm $^{-2}$ s $^{-1}$ )	Intercalibration factors (ISGRI/JEM-X SPI/JEM-X)
$34^{+4}_{-3}$	1.2/100	$9.9 \times 10^{-9}$	$0.94 \pm 0.09$ $0.95^{+0.13}_{-0.09}$

#### REFERENCES

- Baykal, A., Stark, M. J., Swank, J. H. 2002, ApJ, 569, 903
- Blay, P., Reig, P., Martínez Núñez, S., Camero, A., Connell, P., Reglero, V. 2004, in these proceedings
- Bildsten et al. 1997, ApJS, 113, 367
- Bouchet, L., Jourdain, E., Roques, J.P., et al. 2003, A&A, 411, L377
- Coe, M.J., Longmore, A., Payne, B.J., & Hanson, C.G. 1988, MNRAS, 232, 865
- Coe, M.J. 2000, ASP Conference Series, The Be Phenomenon in Early-Type Stars, 214, 656
- Courvoisier, T.J.-L., Walter, R., Beckmann, V., et al. 2003, A&A, 411, L53
- Diehl, R., Baby, N., Beckmann, V. et al. 2003, A&A, 411, L117
- Goldwurm A., David, P., Foschini, L., et al. 2003, A&A, 411, L223

Kuznetsov, S., Falanga, M., Blay, P., Goldwurm, A.,  
Goldoni, P., Reglero, V. 2003, A&A, 411, L437

Kuznetsov, S. et al. 2004, in these proceedings

Lubiński, P., Dubath, P., Kretschmar, P., et al. 2004, these  
proceedings, astro-ph/0405460

Lund, N., Brandt, S., Budtz-Joergensen C., et al. 2003,  
A&A , 411, L411

Martínez Núñez, S., Reig, P., Blay, P., Kretschmar, P.,  
Lund, N., Reglero, V. 2003, A&A, 411, L411

Motch , C., & Janot-Pacheco, E. 1987, A&A, 182, L55

Reig, P., & Coe, M. J. 1998, MNRAS, 294, 118

Reig, P., Stevens, J. B., Coe, M. J., Fabregat, J. 1988,  
MNRAS, 301, 42

Reig, P., & Coe, M. J. 1999, MNRAS, 302, 700

Reynolds, A.P, Parmar, A.N, & White, N.E. 1993, ApJ,  
414, 302

Parmar, A.N, White, N.E., Stella, L., Izzo, C., & Ferri P.  
1989, ApJ, 338, 359

Stollberg, M.T., Finger, M. H., Wilson, R.B., et al. 1999,  
ApJ, 512, 313

Ubertini, P., Lebrun, F., Di Cocco, G., et al. 2003, A&A,  
411, L131

Vedrenne, G., Roques, J.-P., Schönfelder, V., et al. 2002,  
A&A, L411

Westergaard, N.J., Kretschmar, P., Oxborrow, C.A., et al.  
2003, A&A, 411, L257

Wilson, C.A., Finger, M. H., Coe, M. J., et al. 2002, ApJ,  
570, 287

Winkler, C., Courvoisier, T. J.-L., Di Cocco, G., et al.  
2003, A&A, L411